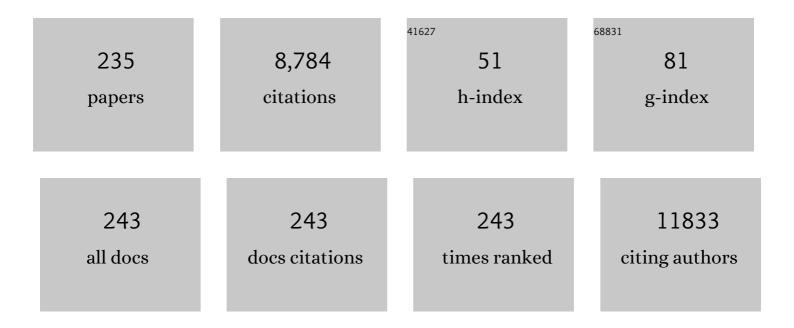
List of Publications by Year in descending order

Source: https://exaly.com/author-pdf/5145376/publications.pdf Version: 2024-02-01



	Πεγαν	HE	
ŧ	Article	IF	CITATIONS
	Improved comprehensive performance of CsPbI2Br perovskite solar cells by modifying the photoactive layers with carbon nanodots. Journal of Materiomics, 2022, 8, 358-365.	2.8	13

## 

3	High-performance aqueous asymmetric supercapacitors based on the cathode of one-step electrodeposited cracked bark-shaped nickel manganese sulfides on activated carbon cloth. Science China Technological Sciences, 2022, 65, 293-301.	2.0	11
4	Synergetic effects of a front ITO nanocylinder array and a back square Al array to enhance light absorption for organic solar cells. Applied Optics, 2022, 61, 1726.	0.9	2
5	Ion-Selective Covalent Organic Framework Membranes as a Catalytic Polysulfide Trap to Arrest the Redox Shuttle Effect in Lithium–Sulfur Batteries. ACS Applied Materials & Interfaces, 2022, 14, 4079-4090.	4.0	32
6	To achieve controlled specific capacities of silicon-based anodes for high-performance lithium-ion batteries. Journal of Alloys and Compounds, 2022, 905, 164189.	2.8	14
7	Sheet-Like Stacking SnS <sub>2</sub> /rGO Heterostructures as Ultrastable Anodes for Lithium-Ion Batteries. ACS Applied Materials & Interfaces, 2022, 14, 11739-11749.	4.0	28
8	The Synergy of La <sub>2</sub> O <sub>3</sub> Nanoparticles and Graphene for Advanced Li Batteries. ChemistrySelect, 2022, 7, .	0.7	1
9	Mn(OH)2-coated Ni3S2 nanosheets on Ni foam as a cathode for high-performance aqueous asymmetric supercapacitors. Journal of Energy Storage, 2022, 51, 104513.	3.9	16
10	Resistive Switching Memristor: On the Direct Observation of Physical Nature of Parameter Variability. ACS Applied Materials & Interfaces, 2022, 14, 1557-1567.	4.0	6
11	One-step electrodeposited Co and Mn layered double hydroxides on Ni foam for high-performance aqueous asymmetric supercapacitors. Journal of Energy Storage, 2022, 50, 104667.	3.9	16
12	NaBr-Modified CsPbl <sub>2</sub> Br Improves the Comprehensive Performance of the Solar Cells. IEEE Journal of Photovoltaics, 2022, 12, 948-953.	1.5	6
13	Solution-Processed Back-Contact PEDOT:PSS/n-Si Heterojunction Solar Cells. ACS Applied Energy Materials, 2022, 5, 5502-5507.	2.5	4
14	Enhanced immobilization and accelerated conversion of polysulfides by functionalized separator for advanced lithium sulfur batteries. Journal of Power Sources, 2022, 539, 231490.	4.0	6
15	High-Performance Osmotic Power Generators Based on the 1D/2D Hybrid Nanochannel System. ACS Applied Materials & Interfaces, 2022, 14, 29197-29212.	4.0	7
16	SnCl <sub>4</sub> -Treated Ti <sub>3</sub> C <sub>2</sub> T <sub><i>x</i></sub> MXene Nanosheets for Schottky Junction Solar Cells with Improved Performance. ACS Applied Nano Materials, 2022, 5, 10064-10072.	2.4	6
17	CeO2 decorated graphene as separator modification material for capture and boost conversion of polysulfide in lithium-sulfur batteries. Journal of Membrane Science, 2021, 619, 118780.	4.1	55
18	High photosensitivity light-controlled planar ZnO artificial synapse for neuromorphic computing. Nanoscale, 2021, 13, 2502-2510.	2.8	25

#

#	Article	IF	CITATIONS
19	Sandwich-like SnS <sub>2</sub> /graphene multilayers for efficient lithium/sodium storage. Dalton Transactions, 2021, 50, 14884-14890.	1.6	6
20	MXenes for Solar Cells. Nano-Micro Letters, 2021, 13, 78.	14.4	90
21	Interconnected Vertical δ-MnO <sub>2</sub> Nanoflakes Coated by a Dopamine-Derived Carbon Thin Shell as a High-Performance Self-Supporting Cathode for Aqueous Zinc Ion Batteries. Journal of the Electrochemical Society, 2021, 168, 030540.	1.3	19
22	One-step construction of δ-MnO2 cathodes with an interconnected nanosheet structure on graphite paper for high-performance aqueous asymmetric supercapacitors. Journal of Energy Storage, 2021, 35, 102308.	3.9	17
23	Twenty Percent Efficiency Crystalline Silicon Solar Cells with Solution-Processed Electron-Selective Contacts. ACS Applied Energy Materials, 2021, 4, 3644-3650.	2.5	8
24	Improvement of the Optoelectrical Properties of a Transparent Conductive Polymer via the Introduction of ITO Nanoparticles and Its Application in Crystalline Silicon/Organic Heterojunction Solar Cells. ACS Applied Materials & Interfaces, 2021, 13, 31171-31179.	4.0	5
25	High-Mass-Loading Ni–Co–S Electrodes with Unfading Electrochemical Performance for Supercapacitors. ACS Applied Energy Materials, 2021, 4, 6531-6541.	2.5	32
26	Enhanced electrochemical performance of lithium-sulfur batteries using a V2O5/graphene interlayer. Journal of Alloys and Compounds, 2021, 868, 159131.	2.8	21
27	Effects of heavy ion irradiation on Cu/Al2O3/Pt CBRAM devices. Microelectronic Engineering, 2021, 247, 111600.	1.1	6
28	Fabricating a Carbon Microtube Interlayer by a Sustainable Green Process as a Polysulfide-Trapping Shield for Lithium-Sulfur Batteries. Energy & Fuels, 2021, 35, 14140-14147.	2.5	6
29	Improvement of electrochemical performances of ultrathin Ti-coated Si-based multilayer nanofibers as anode materials for lithium-ion batteries. Surface and Coatings Technology, 2021, 424, 127669.	2.2	6
30	Cracked bark-inspired ternary metallic sulfide (NiCoMnS4) nanostructure on carbon cloth for high-performance aqueous asymmetric supercapacitors. Science China Materials, 2021, 64, 1632-1641.	3.5	32
31	NiCo2O4 nanowire-supported NiCoMnS4 nanosheets on carbon cloth as a flexible cathode for high-performance aqueous supercapacitors. Electrochimica Acta, 2021, 398, 139324.	2.6	24
32	High-Efficiency Si/PEDOT:PSS Hybrid Heterojunction Solar Cells Using Solution-Processed Graphene Oxide as an Antireflection and Inversion-Induced Layer. ACS Applied Energy Materials, 2021, 4, 13279-13287.	2.5	5
33	Carbon nanotubes@Ni3V2O8@NiCo2S4 nanosheets on Ni foam as a cathode for high-performance aqueous supercapacitors. Journal of Energy Storage, 2021, 44, 103496.	3.9	20
34	A highly stable and sensitive ethanol sensor based on Ru-decorated 1D WO <sub>3</sub> nanowires. RSC Advances, 2021, 11, 39130-39141.	1.7	11
35	Poly(3,4-ethylenedioxythiophene)–Polystyrenesulfonate-Added Layered Vanadium Oxide Cathode for High-Performance Zinc-Ion Batteries. ACS Applied Energy Materials, 2021, 4, 14582-14589.	2.5	11
36	Interconnected δ-MnO2 nanosheets anchored on activated carbon cloth as flexible electrode for high-performance aqueous asymmetric supercapacitors. Journal of Electroanalytical Chemistry, 2020, 877, 114656.	1.9	44

#	Article	IF	CITATIONS
37	Bridging for Carriers by Embedding Metal Oxide Nanoparticles in the Photoactive Layer to Enhance Performance of Polymer Solar Cells. IEEE Journal of Photovoltaics, 2020, 10, 1353-1358.	1.5	16
38	Robust Polyethylenimine Electrolyte for High Performance and Thermally Stable Atomic Switch Memristors. Advanced Functional Materials, 2020, 30, 2004514.	7.8	31
39	TiO <sub>2</sub> Nanoparticles In Situ Formed on Ti <sub>3</sub> C <sub>2</sub> Nanosheets by a One‣tep Ethanolâ€Thermal Method for Enhanced Reversible Lithiumâ€ion Storage. ChemistrySelect, 2020, 5, 3124-3129.	0.7	21
40	Improvement of the Optoelectrical Properties of a Transparent Conductive Polymer via a Simple Mechanical Pressure Treatment. ACS Omega, 2020, 5, 7545-7554.	1.6	5
41	Cr-Doped Urchin-Like WO3 Hollow Spheres: The Cooperative Modulation of Crystal Growth and Energy-Band Structure for High-Sensitive Acetone Detection. Sensors, 2020, 20, 3473.	2.1	26
42	Enhanced performance and the related mechanisms of organic solar cells using Li-doped SnO2 as the electron transport layer. Materials Chemistry and Physics, 2020, 254, 123536.	2.0	9
43	Effects of high energy heavy ion irradiation on resistive switches. Microelectronic Engineering, 2020, 231, 111393.	1.1	3
44	Controlled Growth of Fine Multifilaments in Polymer-Based Memristive Devices Via the Conduction Control. ACS Applied Materials & amp; Interfaces, 2020, 12, 34370-34377.	4.0	23
45	SiO <sub>2</sub> /Ta <sub>2</sub> O <sub>5</sub> heterojunction ECM memristors: physical nature of their low voltage operation with high stability and uniformity. Nanoscale, 2020, 12, 4320-4327.	2.8	24
46	Resistive switching behaviors and mechanisms of HfS2 film memory devices studied by experiments and density functional theory calculations. Applied Physics Letters, 2020, 116, .	1.5	5
47	A Hierarchical Interconnected Nanosheet Structure of Porous δ-MnO <sub>2</sub> on Graphite Paper as Cathode with a Broad Potential Window for NaNO <sub>3</sub> Aqueous Electrolyte Supercapacitors. ACS Applied Energy Materials, 2020, 3, 2614-2622.	2.5	32
48	Nb <sub>2</sub> O <sub>5</sub> /RGO Nanocomposite Modified Separators with Robust Polysulfide Traps and Catalytic Centers for Boosting Performance of Lithium–Sulfur Batteries. Small, 2019, 15, e1902363.	5.2	83
49	Wider Voltage Window, High Capacity and Ultraâ€Long Life of an Na 0.91 MnO 2 Cathode for an Aqueous Highâ€Performance Supercapacitor. Batteries and Supercaps, 2019, 2, 948-955.	2.4	7
50	Large-scale self-template synthesis of NiCo2O4 nanotubes derived from alginate for high-rate lithium storage properties stimulated by capacitive effects. Journal of Alloys and Compounds, 2019, 810, 151736.	2.8	12
51	Hole selective materials and device structures of heterojunction solar cells: Recent assessment and future trends. APL Materials, 2019, 7, .	2.2	27
52	Pseudocapacitive reaction enhanced porous Co0.85Se/N-doped carbon anodes for advanced sodium-ion battery with high rate and capacity. Electrochimica Acta, 2019, 321, 134643.	2.6	16
53	Enhanced performance of polymer solar cells by adding SnO2 nanoparticles in the photoactive layer. Organic Electronics, 2019, 73, 7-12.	1.4	21
54	Mesoporous boron carbon nitride/graphene modified separators as efficient polysulfides barrier for highly stable lithium-sulfur batteries. Journal of Electroanalytical Chemistry, 2019, 842, 34-40.	1.9	24

#	Article	IF	CITATIONS
55	A Novel Strategy for the Selection of Polysulfide Adsorbents Toward Highâ€Performance Lithiumâ€&ulfur Batteries. Advanced Materials Interfaces, 2019, 6, 1900393.	1.9	7
56	High mass loading Ni-decorated Co9S8 with enhanced electrochemical performance for flexible quasi-solid-state asymmetric supercapacitors. Journal of Power Sources, 2019, 423, 106-114.	4.0	48
57	2.5 V salt-in-water supercapacitors based on alkali type double salt/carbon composite anode. Journal of Materials Chemistry A, 2019, 7, 26011-26019.	5.2	16
58	Resistive switching behaviors mediated by grain boundaries in one longitudinal Al/MoS2&PVP/ITO device. Materials Science in Semiconductor Processing, 2019, 91, 246-251.	1.9	11
59	Fe3O4/RGO modified separators to suppress the shuttle effect for advanced lithium-sulfur batteries. Journal of Alloys and Compounds, 2019, 784, 149-156.	2.8	61
60	Enhanced electrochemical kinetics in lithium-sulfur batteries by using carbon nanofibers/manganese dioxide composite as a bifunctional coating on sulfur cathode. Electrochimica Acta, 2018, 269, 180-187.	2.6	62
61	Sulfur Immobilizer by Nanoscale TiO <sub>2</sub> Trapper Deposited on Hierarchical Porous Carbon and Graphene for Cathodes of Lithium–Sulfur Batteries. Advanced Materials Interfaces, 2018, 5, 1701602.	1.9	24
62	High-performance free-standing capacitor electrodes of multilayered Co9S8 plates wrapped by carbonized poly(3,4-ethylenedioxythiophene):poly(styrene sulfonate)/reduced graphene oxide. Journal of Power Sources, 2018, 379, 167-173.	4.0	59
63	High-yield fabrication of graphene-wrapped silicon nanoparticles for self-support and binder-free anodes of lithium-ion batteries. Journal of Alloys and Compounds, 2018, 744, 243-251.	2.8	17
64	MoS2/Ni3S4 composite nanosheets on interconnected carbon shells as an excellent supercapacitor electrode architecture for long term cycling at high current densities. Applied Surface Science, 2018, 440, 741-747.	3.1	49
65	Excellent Light Confinement of Hemiellipsoid- and Inverted Hemiellipsoid-Modified Semiconductor Nanowire Arrays. Nanoscale Research Letters, 2018, 13, 236.	3.1	6
66	Oxygen vacancy drift controlled three-terminal ReRAM with a reduction in operating gate bias and gate leakage current. Solid State Ionics, 2018, 328, 30-34.	1.3	3
67	Modulation-doped ZnO as high performance electron-selective layer for efficient silicon heterojunction solar cells. Nano Energy, 2018, 54, 99-105.	8.2	34
68	Flexible all-solid-state ultrahigh-energy asymmetric supercapacitors based on tailored morphology of NiCoO <sub>2</sub> /Ni(OH) <sub>2</sub> /Co(OH) <sub>2</sub> electrodes. CrystEngComm, 2018, 20, 6519-6528.	1.3	14
69	Hollow irregular octahedra-like NiCo2O4 cages composed of mesoporous nanosheets as a superior anode material for lithium-ion batteries. Chemical Engineering Journal, 2018, 350, 29-36.	6.6	39
70	Selfâ€ <b>5</b> upport Surface Enhanced Raman Scattering Substrates with the Function of Enriching Analytes. Advanced Materials Interfaces, 2018, 5, 1800559.	1.9	1
71	A Dual Carbonâ€Based Potassium Dual Ion Battery with Robust Comprehensive Performance. Small, 2018, 14, e1801836.	5.2	118
72	Molybdenum disulfide nanosheets embedded in hollow nitrogen-doped carbon spheres for efficient lithium/sodium storage with enhanced electrochemical kinetics. Electrochimica Acta, 2018, 283, 646-654.	2.6	24

#	Article	IF	CITATIONS
73	A low crystallinity oxygen-vacancy-rich Co <sub>3</sub> O <sub>4</sub> cathode for high-performance flexible asymmetric supercapacitors. Journal of Materials Chemistry A, 2018, 6, 16094-16100.	5.2	182
74	Carbon fabric supported 3D cobalt oxides/hydroxide nanosheet network as cathode for flexible all-solid-state asymmetric supercapacitor. Dalton Transactions, 2018, 47, 11503-11511.	1.6	34
75	Rapid activation and enhanced cycling stability of Co3O4 microspheres decorated by N-doped amorphous carbon shell for advanced LIBs. Electrochimica Acta, 2018, 283, 979-986.	2.6	36
76	Polydopamine derived porous N-doped carbon nanofibers for lithium ion storage. Materials Letters, 2017, 189, 259-262.	1.3	8
77	Self-supported binder-free carbon fibers/MnO 2 electrodes derived from disposable bamboo chopsticks for high-performance supercapacitors. Journal of Alloys and Compounds, 2017, 699, 126-135.	2.8	60
78	High performance silicon–organic hybrid solar cells via improving conductivity of PEDOT:PSS with reduced graphene oxide. Applied Surface Science, 2017, 407, 398-404.	3.1	51
79	Synthesis and lithium storage properties of interconnected fullerene-like carbon nanofibers encapsulated with tin nanoparticles. Journal of Materials Science, 2017, 52, 6969-6975.	1.7	7
80	The effect of oxygen vacancy on switching mechanism of ZnO resistive switching memory. Applied Physics Letters, 2017, 110, .	1.5	79
81	Wrinkled-paper-like ZnCo 2 O 4 nanoflakes as a superior anode material for ultrahigh-rate lithium-ion batteries. Journal of Alloys and Compounds, 2017, 711, 592-597.	2.8	20
82	Time-decay Memristive Behavior and diffusive dynamics in one forget process operated by a 3D vertical Pt/Ta2O5â^'x/W device. Scientific Reports, 2017, 7, 822.	1.6	12
83	Nanoscale α-MnS crystallites grown on N-S co-doped rGO as a long-life and high-capacity anode material of Li-ion batteries. Applied Surface Science, 2017, 416, 858-867.	3.1	66
84	Size-controllable porous NiO electrodes for high-performance lithium ion battery anodes. Materials Research Bulletin, 2017, 96, 533-537.	2.7	28
85	Interfacial modification of a lightweight carbon foam current collector for high-energy density Si/LCO lithium-ion batteries. Journal of Materials Chemistry A, 2017, 5, 13168-13175.	5.2	35
86	Nanostructural optimization of silicon/PEDOT:PSS hybrid solar cells for performance improvement. Journal Physics D: Applied Physics, 2017, 50, 175105.	1.3	18
87	Facile synthesis of ultrathin NiCo <sub>2</sub> S <sub>4</sub> nano-petals inspired by blooming buds for high-performance supercapacitors. Journal of Materials Chemistry A, 2017, 5, 7144-7152.	5.2	251
88	Effect of rGO Coating on Interconnected Co3O4 Nanosheets and Improved Supercapacitive Behavior of Co3O4/rGO/NF Architecture. Nano-Micro Letters, 2017, 9, 38.	14.4	67
89	High-performanceÂSi/organic hybrid solar cells using a novel cone-shaped Si nanoholes structures and back surface passivation layer. Nano Energy, 2017, 41, 519-526.	8.2	18
90	Group IVA Element (Si, Ge, Sn)â€Based Alloying/Dealloying Anodes as Negative Electrodes for Fullâ€Cell Lithiumâ€Ion Batteries. Small, 2017, 13, 1702000.	5.2	163

#	Article	IF	CITATIONS
91	Dual functional MoS2/graphene interlayer as an efficient polysulfide barrier for advanced lithium-sulfur batteries. Electrochimica Acta, 2017, 256, 28-36.	2.6	106
92	Facile embedding of SiO2 nanoparticles in organic solar cells for performance improvement. Organic Electronics, 2017, 50, 77-81.	1.4	25
93	Wellâ€Designed Hierarchical Co <sub>3</sub> O <sub>4</sub> Architecture as a Longâ€Life and Ultrahigh Rate Capacity Anode for Advanced Lithiumâ€Ion Batteries. Advanced Materials Interfaces, 2017, 4, 1700553.	1.9	37
94	Greatly improved cyclability for Li-ion batteries with a PEDOT–PSS coated nanostructured Ge anode. Surfaces and Interfaces, 2017, 8, 214-218.	1.5	14
95	Flexible and Wearable Allâ€Solidâ€State Supercapacitors with Ultrahigh Energy Density Based on a Carbon Fiber Fabric Electrode. Advanced Energy Materials, 2017, 7, 1700409.	10.2	169
96	Inner porous carbon nanofibers as binder-free electrodes for high-rate supercapacitors. Electrochimica Acta, 2017, 258, 1064-1071.	2.6	20
97	Carbon-coated Si nanoparticles/reduced graphene oxide multilayer anchored to nanostructured current collector as lithium-ion battery anode. Applied Surface Science, 2017, 396, 41-47.	3.1	49
98	Carbon-wrapped MnO nanodendrites interspersed on reduced graphene oxide sheets as anode materials for lithium-ion batteries. Applied Surface Science, 2017, 394, 1-8.	3.1	30
99	<i>Inâ€situ</i> stress suppression of hydrogenated aâ€CN <sub>x</sub> film prepared via Ar gas introduction. Surface and Interface Analysis, 2017, 49, 370-375.	0.8	0
100	Wedge-shaped semiconductor nanowall arrays with excellent light management. Optics Letters, 2017, 42, 3928.	1.7	14
101	Fabrication of hybrid Co3O4/NiCo2O4 nanosheets sandwiched by nanoneedles for high-performance supercapacitors using a novel electrochemical ion exchange. Science China Materials, 2017, 60, 1168-1178.	3.5	38
102	Phosphorus-doped silicon nanorod anodes for high power lithium-ion batteries. Beilstein Journal of Nanotechnology, 2017, 8, 222-228.	1.5	11
103	Improved lithium-ion battery anode capacity with a network of easily fabricated spindle-like carbon nanofibers. Beilstein Journal of Nanotechnology, 2016, 7, 1289-1295.	1.5	6
104	Nanostructured semiconductor solar absorbers with near 100% absorption and related light management picture. Journal Physics D: Applied Physics, 2016, 49, 215104.	1.3	11
105	Freestanding flexible graphene foams@polypyrrole@MnO <sub>2</sub> electrodes for high-performance supercapacitors. Journal of Materials Chemistry A, 2016, 4, 9196-9203.	5.2	83
106	Fabrication of voids-involved SnO2@C nanofibers electrodes with highly reversible Sn/SnO2 conversion and much enhanced coulombic efficiency for lithium-ion batteries. Journal of Power Sources, 2016, 327, 21-28.	4.0	80
107	Rational design of hierarchical Ni embedded NiO hybrid nanospheres for high-performance lithium-ion batteries. RSC Advances, 2016, 6, 72008-72014.	1.7	6
108	Vertical graphene nanosheets synthesized by thermal chemical vapor deposition and the field emission properties. Journal Physics D: Applied Physics, 2016, 49, 385301.	1.3	22

#	Article	IF	CITATIONS
109	3D flexible O/N Co-doped graphene foams for supercapacitor electrodes with high volumetric and areal capacitances. Journal of Power Sources, 2016, 336, 455-464.	4.0	54
110	Ferrocene derived core-shell structural Fe 3 O 4 @C nanospheres for superior lithium storage properties. Electrochimica Acta, 2016, 220, 107-113.	2.6	38
111	Facilely scraping Si nanoparticles@reduced graphene oxide sheets onto nickel foam as binder-free electrodes for lithium ion batteries. Electrochimica Acta, 2016, 193, 246-252.	2.6	10
112	Facile fabrication of binder-free NiO electrodes with high rate capacity for lithium-ion batteries. Applied Surface Science, 2016, 368, 298-302.	3.1	35
113	A Low-Stress, Elastic, and Improved Hardness Hydrogenated Amorphous Carbon Film. Journal of Nanomaterials, 2015, 2015, 1-5.	1.5	0
114	Interconnected porous NiO@MnO2 nanosheets as anodes with excellent rate capability for lithium-ion batteries. Materials Letters, 2015, 157, 7-10.	1.3	20
115	DIP-coating process to fabricate SnO2/C nanotube networks as binder-free anodes for lithium ion batteries. Materials Letters, 2015, 158, 244-247.	1.3	6
116	Germanium Anode with Excellent Lithium Storage Performance in a Germanium/Lithium–Cobalt Oxide Lithium-Ion Battery. ACS Nano, 2015, 9, 1858-1867.	7.3	148
117	Facile synthesis of porous Fe3O4@C nanospheres as high-performance anode for lithium-ion battery. Journal of Solid State Electrochemistry, 2015, 19, 1211-1215.	1.2	36
118	Ultra-thick porous films of graphene-encapsulated silicon nanoparticles as flexible anodes for lithium ion batteries. Electrochimica Acta, 2015, 174, 688-695.	2.6	44
119	Electrochemically deposited interconnected porous Co3O4 nanoflakes as anodes with excellent rate capability for lithium ion batteries. RSC Advances, 2015, 5, 36117-36121.	1.7	8
120	N-Doped Amorphous Carbon Coated Fe <sub>3</sub> O <sub>4</sub> /SnO <sub>2</sub> Coaxial Nanofibers as a Binder-Free Self-Supported Electrode for Lithium Ion Batteries. ACS Applied Materials & Interfaces, 2014, 6, 20334-20339.	4.0	82
121	Facile Synthesis of Porous MnO Microspheres for Highâ€Performance Lithiumâ€ion Batteries. Particle and Particle Systems Characterization, 2014, 31, 1001-1007.	1.2	24
122	Facile synthesis of 3D networks of C/SnOx/C hybrid nanofibers with enhanced lithium storage. Materials Letters, 2014, 116, 271-274.	1.3	4
123	High areal capacity Li ion battery anode based on thick mesoporous Co3O4 nanosheet networks. Nano Energy, 2014, 5, 91-96.	8.2	112
124	Preparation and visible-light photocatalytic activity of α-Fe2O3/γ-Fe2O3 magnetic heterophase photocatalyst. Materials Letters, 2014, 118, 107-110.	1.3	45
125	Effect of Zn-substitution on cycling performance of $\hat{I}\pm$ -Co(OH)2 nanosheet electrode for supercapacitors. Journal of Materials Chemistry A, 2014, 2, 2585.	5.2	53
126	Radial junction Si micro/nano-wire array photovoltaics: Recent progress from theoretical investigation to experimental realization. Nano Energy, 2014, 7, 10-24.	8.2	46

#	Article	IF	CITATIONS
127	Copper nanorods supported phosphorus-doped silicon for lithium storage application. Materials Letters, 2014, 117, 58-61.	1.3	19
128	A facile and inexpensive approach to improve the performance of silicon film as an anode for lithium-ion batteries. Journal of Materials Chemistry A, 2014, 2, 14817.	5.2	12
129	Building a Ni <sub>3</sub> S <sub>2</sub> nanotube array and investigating its application as an electrode for lithium ion batteries. Chemical Communications, 2014, 50, 9361-9364.	2.2	84
130	Facile preparation of Mn <sub>3</sub> O <sub>4</sub> -coated carbon nanofibers on copper foam as a high-capacity and long-life anode for lithium-ion batteries. Journal of Materials Chemistry A, 2014, 2, 17352-17358.	5.2	32
131	Facile synthesis of rGO/SnO <sub>2</sub> composite anodes for lithium ion batteries. Journal of Materials Chemistry A, 2014, 2, 17139-17145.	5.2	62
132	Interconnected MnO2 nanoflakes supported by 3D nanostructured stainless steel plates for lithium ion battery anodes. Electrochimica Acta, 2014, 121, 415-420.	2.6	34
133	Preparation and electrochemical performance of MWCNTs@MnO2 nanocomposite for lithium ion batteries. Science China Technological Sciences, 2014, 57, 1077-1080.	2.0	9
134	In situ coating of NiO on Ni-silicide nanowires with roughened surfaces for improved electrochemical energy storage. Journal of Materials Chemistry A, 2014, 2, 9156.	5.2	5
135	Magnetically Assembled Ni@Ag Urchinâ€Like Ensembles with Ultraâ€Sharp Tips and Numerous Gaps for SERS Applications. Small, 2014, 10, 2564-2569.	5.2	18
136	Carbon-Wrapped Fe3O4 Nanoparticle Films Grown on Nickel Foam as Binder-Free Anodes for High-Rate and Long-Life Lithium Storage. ACS Applied Materials & Interfaces, 2014, 6, 648-654.	4.0	60
137	Cermanium anode with lithiated-copper-oxide nanorods as an electronic-conductor for high-performance lithium-ion batteries. Materials Letters, 2014, 136, 107-110.	1.3	16
138	Nitrogen-doped carbon nanofibers as anode material for high-capacity and binder-free lithium ion battery. Materials Letters, 2014, 120, 39-42.	1.3	34
139	Electrochemical performances of nanorod structured Si1â^'xGex anodes. Materials Letters, 2014, 128, 163-166.	1.3	5
140	Flexible free-standing graphene foam supported silicon films as high capacity anodes for lithium ion batteries. Materials Letters, 2014, 128, 132-135.	1.3	32
141	Mesoporous NiO nanosheet networks as high performance anodes for Li ion batteries. Journal of Materials Chemistry A, 2013, 1, 4173.	5.2	259
142	Single electrospun porous NiO–ZnO hybrid nanofibers as anode materials for advanced lithium-ion batteries. Nanoscale, 2013, 5, 3037.	2.8	146
143	Preparation and study of carbon nano-onion for lithium storage. Materials Chemistry and Physics, 2013, 139, 333-337.	2.0	22
144	Study on performance of PVDF piezoelectric film for the separator in Li-ion rechargeable cell. Science China Technological Sciences, 2013, 56, 2646-2648.	2.0	1

#	Article	IF	CITATIONS
145	Growth of nanostructured nickel sulfide films on Ni foam as high-performance cathodes for lithium ion batteries. Physical Chemistry Chemical Physics, 2013, 15, 9924.	1.3	92
146	Template-free synthesized Ni nanofoams as nanostructured current collectors for high-performance electrodes in lithium ion batteries. Journal of Materials Chemistry A, 2013, 1, 10002.	5.2	36
147	Synthesis, characterization, and lithium-storage of ZnO–SnO2 hierarchical architectures. RSC Advances, 2013, 3, 7758.	1.7	32
148	Network structures of fullerene-like carbon core/nano-crystalline silicon shell nanofibers as anode material for lithium-ion batteries. Carbon, 2013, 54, 29-35.	5.4	53
149	Self-combustion fabrication of anatase/rutile titanium oxides encapsulated in thin carbon shells and their photocatalytic performance. Materials Letters, 2013, 113, 163-166.	1.3	3
150	Ultrathin nanoporous Fe3O4–carbon nanosheets with enhanced supercapacitor performance. Journal of Materials Chemistry A, 2013, 1, 1952.	5.2	168
151	Three-dimensional network structured α-Fe2O3 made from a stainless steel plate as a high-performance electrode for lithium ion batteries. Journal of Materials Chemistry A, 2013, 1, 6400.	5.2	148
152	Preparation of 3D nanoporous copper-supported cuprous oxide for high-performance lithium ion battery anodes. Nanoscale, 2013, 5, 1917.	2.8	91
153	A new carbonaceous material derived from biomass source peels as an improved anode for lithium ion batteries. Journal of Analytical and Applied Pyrolysis, 2013, 100, 181-185.	2.6	88
154	Facile synthesis of CuO nanorod for lithium storage application. Materials Letters, 2013, 90, 4-7.	1.3	57
155	Synthesis of core–shell architectures of silicon coated on controllable grown Ni-silicide nanostructures and their lithium-ion battery application. CrystEngComm, 2013, 15, 7298.	1.3	24
156	Self-supporting Co3O4 with lemongrass-like morphology as a high-performance anode material for lithium ion batteries. Journal of Materials Chemistry, 2012, 22, 17429.	6.7	75
157	Interconnected porous MnO nanoflakes for high-performance lithium ion battery anodes. Journal of Materials Chemistry, 2012, 22, 9189.	6.7	169
158	Preparation of nano-networks of MnO <sub>2</sub> shell/Ni current collector core for high-performance supercapacitor electrodes. Journal of Materials Chemistry, 2012, 22, 483-487.	6.7	86
159	Electrochemical behaviors of porous SnO2–Sn/C composites derived from pyrolysis of SnO2/poly(vinylidene fluoride). Electrochimica Acta, 2012, 66, 204-209.	2.6	89
160	Synthesis of novel pompon-like porous SnO2 and its application in lithium-ion battery. Materials Letters, 2012, 66, 193-195.	1.3	26
161	Synthesis of monodisperse single crystal Zn2SnO4 cubes with high lithium storage capacity. Materials Letters, 2012, 76, 66-68.	1.3	44
162	Nanostructured NiO electrode for high rate Li-ion batteries. Journal of Materials Chemistry, 2011, 21, 3571.	6.7	330

#	Article	IF	CITATIONS
163	NiO nanocone array electrode with high capacity and rate capability for Li-ion batteries. Journal of Materials Chemistry, 2011, 21, 9988.	6.7	194
164	Broadband antireflection of silicon nanorod arrays prepared by plasma enhanced chemical vapor deposition. Applied Surface Science, 2011, 258, 1058-1061.	3.1	6
165	Hydrothermal synthesis of Cu3(OH)2V2O7•nH2O nanoparticles and its application in lithium ion battery. Journal of Alloys and Compounds, 2011, 509, L142-L144.	2.8	14
166	Low temperature synthesis of Fe3O4 micro-spheres and its application in lithium ion battery. Journal of Alloys and Compounds, 2011, 509, L305-L307.	2.8	23
167	Effects of the distance between the inductance coil and substrates on the microstructure and optical properties of silicon films deposited by ICP-CVD. Physics Procedia, 2011, 18, 128-135.	1.2	1
168	Low temperature synthesis of Fe3O4 nanoparticles and its application in lithium ion batteries. Materials Chemistry and Physics, 2011, 130, 1260-1264.	2.0	8
169	The structure and optical properties of silicon nanowires prepared by inductively coupled plasma chemical vapor deposition. Materials Letters, 2011, 65, 1117-1119.	1.3	15
170	Improved performance for lithium-ion batteries with nickel nanocone-arrays supported germanium anode. Materials Letters, 2011, 65, 1542-1544.	1.3	12
171	Performance of Si–Ni nanorod as anode for Li-ion batteries. Materials Letters, 2011, 65, 3227-3229.	1.3	22
172	Visible photoluminescence of hydrothermal synthesized Sn1â^'x Ni x O2 nanostructures. Journal of Materials Science: Materials in Electronics, 2011, 22, 174-178.	1.1	3
173	The microstructure and optical properties of crystallized hydrogenated silicon films prepared by very high frequency glow discharge. Applied Surface Science, 2011, 257, 8350-8354.	3.1	16
174	Highly water-soluble nanocrystal powders of magnetite and maghemite coated with gluconic acid: Preparation, structure characterization, and surface coordination. Journal of Colloid and Interface Science, 2011, 354, 76-81.	5.0	29
175	Ultraviolet photoconductance of a single hexagonal WO3 nanowire. Nano Research, 2010, 3, 281-287.	5.8	127
176	W18O49 Nanowires as Ultraviolet Photodetector. Nanoscale Research Letters, 2010, 5, 416-419.	3.1	25
177	Synthesis of Zn3(OH)2V2O7·nH2O hierarchical nanostructures and their photoluminescence properties. Materials Chemistry and Physics, 2010, 120, 426-430.	2.0	11
178	Low temperature synthesis of Fe3O4 micro-spheres and its microwave absorption properties. Materials Chemistry and Physics, 2010, 124, 353-358.	2.0	96
179	Optical properties of Zn3(OH)2V2O7·nH2O nanosheets. Materials Chemistry and Physics, 2010, 124, 803-808.	2.0	10
180	Hydrothermal synthesis and magnetic property of Cu3(OH)2V2O7•nH2O. Materials Letters, 2010, 64, 516-519.	1.3	18

#	Article	IF	CITATIONS
181	Facile synthesis of ultra-long α-MnO2 nanowires and their microwave absorption properties. Materials Letters, 2010, 64, 1496-1498.	1.3	58
182	The optoelectronic properties of silicon films deposited by inductively coupled plasma CVD. Applied Surface Science, 2010, 257, 817-822.	3.1	14
183	The effect of Ar flow rate in the growth of SiGe:H thin films by PECVD. Applied Surface Science, 2010, 256, 7032-7036.	3.1	6
184	Effect of Ar in the source gas on the microstructure and optoelectronic properties of microcrystalline silicon films deposited by plasma-enhanced CVD. Applied Surface Science, 2010, 257, 1342-1346.	3.1	12
185	Designed synthesis of wide range microwave absorption Fe3O4–carbon sphere composite. Journal of Alloys and Compounds, 2010, 489, 252-256.	2.8	98
186	Crystallized Zn3(VO4)2: Synthesis, characterization and optical property. Journal of Alloys and Compounds, 2010, 491, 378-381.	2.8	85
187	The influence of H2/Ar ratio on Ge content of the μc-SiGe:H films deposited by PECVD. Journal of Alloys and Compounds, 2010, 504, 403-406.	2.8	17
188	Hydrothermal synthesis of Zn3(OH)2V2O7·nH2O nanosheets and its application in lithium ion battery. Materials Letters, 2009, 63, 2459-2461.	1.3	32
189	Hydrothermal synthesis of Fe3O4 nanoparticles and its application in lithium ion battery. Materials Letters, 2009, 63, 2701-2703.	1.3	85
190	High temperature dependence of the cubic phase content and optical properties of BN thin films. Surface and Coatings Technology, 2009, 203, 1220-1224.	2.2	2
191	The influence of H2/(H2+Ar) ratio on microstructure and optoelectronic properties of microcrystalline silicon films deposited by plasma-enhanced CVD. Applied Surface Science, 2009, 255, 8867-8873.	3.1	12
192	Crystallized Zn3(OH)2V2O7·nH2O: Hydrothermal synthesis and magnetic property. Journal of Alloys and Compounds, 2009, 477, L1-L3.	2.8	28
193	Low-temperature deposition of highly crystallized silicon films on Al-coated polyethylene napthalate by inductively coupled plasma CVD. Journal of Alloys and Compounds, 2009, 481, 278-282.	2.8	2
194	Synthesis of sheaf-like CuO from aqueous solution and their application in lithium-ion batteries. Journal of Alloys and Compounds, 2009, 484, 322-326.	2.8	41
195	Hydrothermal synthesis and microwave absorption properties of Fe <sub>3</sub> O <sub>4</sub> nanocrystals. Journal Physics D: Applied Physics, 2009, 42, 055004.	1.3	130
196	AlCl3-induced crystallization of amorphous silicon thin films. Applied Surface Science, 2008, 254, 2605-2608.	3.1	2
197	Kinetic Monte Carlo simulation of film morphologies at the initial stages. Science in China Series G: Physics, Mechanics and Astronomy, 2008, 51, 56-63.	0.2	1
198	Raman spectrum of vanadium pentoxide from densityâ€functional perturbation theory. Journal of Raman Spectroscopy, 2008, 39, 1475-1481.	1.2	47

#	Article	IF	CITATIONS
199	Highly crystallized silicon films grown on glass without amorphous incubation layers by inductively coupled plasma chemical vapor deposition. Journal of Crystal Growth, 2008, 310, 4340-4344.	0.7	11
200	Phase transformation in BN films by nitrogen-protected annealing at atmospheric pressure. Applied Surface Science, 2008, 254, 7109-7113.	3.1	18
201	Stress relief patterns of hydrogenated amorphous carbon films grown by dc-pulse plasma chemical vapor deposition. Applied Surface Science, 2008, 255, 1836-1840.	3.1	9
202	The catalyst-free synthesis of large-area tungsten oxide nanowire arrays on ITO substrate and field emission properties. Materials Research Bulletin, 2008, 43, 919-925.	2.7	30
203	Synthesis of flower- and rod-like nickel sulfide nanostructures by an organic-free hydrothermal process. Materials Research Bulletin, 2008, 43, 1440-1447.	2.7	35
204	Controllable synthesis of hexagonal WO <sub>3</sub> nanostructures and their application in lithium batteries. Journal Physics D: Applied Physics, 2008, 41, 155417.	1.3	149
205	Polycrystalline Silicon–Germanium Films Prepared by Aluminum-Induced Crystallization. Journal of the Electrochemical Society, 2008, 155, H903.	1.3	2
206	Deposition of controllable preferred orientation silicon films on glass by inductively coupled plasma chemical vapor deposition. Journal of Applied Physics, 2008, 103, 043505.	1.1	29
207	The evolution of the structure and mechanical properties of fullerenelike hydrogenated amorphous carbon films upon annealing. Journal of Applied Physics, 2008, 104, .	1.1	13
208	The correlation between pentatomic and heptatomic carbon rings and stress of hydrogenated amorphous carbon films prepared by dc-pulse plasma chemical vapor deposition. Applied Physics Letters, 2008, 93, .	1.5	18
209	Fullerene nanostructure-induced excellent mechanical properties in hydrogenated amorphous carbon. Applied Physics Letters, 2007, 91, 141902.	1.5	99
210	Growth and field emission of tungsten oxide nanotip arrays on ITO glass substrate. Applied Surface Science, 2007, 253, 8923-8927.	3.1	19
211	Optical, electrochemical and structural properties of long-term cycled tungsten oxide films prepared by sol–gel. Physica B: Condensed Matter, 2007, 396, 164-168.	1.3	18
212	Deposition and field emission properties of highly crystallized silicon films on aluminum-coated polyethylene napthalate. Journal of Crystal Growth, 2007, 306, 1-5.	0.7	8
213	Study on the initial growth process of crystalline silicon films on aluminum-coated polyethylene napthalate by Raman spectroscopy. Journal of Crystal Growth, 2007, 308, 330-333.	0.7	8
214	Fabrication and photoluminescence properties of large-scale hierarchical CdS dendrites. Materials Letters, 2007, 61, 4773-4776.	1.3	31
215	Low-temperature metal-induced crystallization of hydrogenated amorphous Si1-xGex (0.25â‰竊‰犂) thin films with Au solution. Applied Physics A: Materials Science and Processing, 2007, 90, 267-271.	1.1	3
216	Significant suppression of leakage current in (Ba x ,Sr1-x )TiO3/MgO heterostructured thin films by thin MgO layers insertion. Journal of Sol-Gel Science and Technology, 2007, 42, 9-12.	1.1	9

#	Article	IF	CITATIONS
217	Electron field emission from nano-crystalline Si films deposited by inductively coupled plasma CVD at room temperature. Science Bulletin, 2006, 51, 510-514.	1.7	1
218	Kinetic Monte Carlo simulation of Cu thin film growth. Vacuum, 2004, 72, 405-410.	1.6	58
219	A computer simulation of nucleation and growth of thin films. Computational Materials Science, 2004, 30, 331-336.	1.4	17
220	NANOCRYSTALLINE DIAMOND THIN FILMS AS INFRARED OPTICAL PROTECTIVE COATINGS. International Journal of Modern Physics B, 2002, 16, 1013-1017.	1.0	12
221	PREPARATION OF NANOCRYSTALLINE DIAMOND FIELD EMITTERS USING POROUS SILICON AS HOST MATRIXES. International Journal of Modern Physics B, 2002, 16, 998-1002.	1.0	1
222	INTENSE ROOM-TEMPERATURE PHOTOLUMINESCENCE FROM NANOCRYSTALLINE Ge/SiO2 MULTILAYER STRUCTURES. International Journal of Modern Physics B, 2002, 16, 4238-4241.	1.0	2
223	FORMATION OF OXYGEN-FREE GADOLINIUM SILICIDE LAYER BY ION IMPLANTATION AND PULSED EXCIMER LASER IRRADIATION. International Journal of Modern Physics B, 2002, 16, 4331-4334.	1.0	1
224	Formation of Ytterbium Silicide Thin Films by Solid-Phase Crystallization. Physica Status Solidi A, 2002, 191, 143-148.	1.7	0
225	Relief of the internal stress in ternary boron carbonitride thin films. Applied Surface Science, 2002, 191, 338-343.	3.1	17
226	Ternary BCN thin films deposited by reactive sputtering. Thin Solid Films, 2000, 375, 247-250.	0.8	39
227	Structure of Polycrystalline Silicon Thin Film Fabricated from Fluorinated Precursors by Layer-by-Layer Technique. Japanese Journal of Applied Physics, 1994, 33, 51-56.	0.8	33
228	Carrier transport in polycrystalline silicon films deposited by a layerâ€byâ€layer technique. Journal of Applied Physics, 1994, 76, 4728-4733.	1.1	30
229	Carrier transport and structural properties of polysilicon films prepared by layer-by-layer technique. Solar Energy Materials and Solar Cells, 1994, 34, 271-276.	3.0	7
230	Preparation of High-Quality Microcrystalline Silicon from Fluorinated Precursors by a Layer-by-Layer Technique. Japanese Journal of Applied Physics, 1993, 32, 1539-1545.	0.8	51
231	Structural and Electrical Properties of n-Type Poly-Si Films Prepared by Layer-by-Layer Technique. Japanese Journal of Applied Physics, 1993, 32, 3370-3375.	0.8	14
232	In situ electron spin resonance measurements of thermally induced metastable defects in doped hydrogenated amorphous silicon carbon films. Journal of Non-Crystalline Solids, 1989, 114, 657-659.	1.5	2
233	Hydrogen and boron concentrations in doped hydrogenated amorphous silicon arbon films measured by nuclear reaction analysis. Applied Physics Letters, 1989, 54, 1995-1996.	1.5	2
234	Interface Defects in Sputtered aâ€&i:H/aâ€C:H Multilayers. Physica Status Solidi (B): Basic Research, 1987, 142, K35.	0.7	0

#	Article	IF	CITATIONS
235	Solutionâ€Processed Organic/pâ€Type Silicon Hybrid Heterojunction Solar Cells. Physica Status Solidi - Rapid Research Letters, 0, , 2000560.	1.2	4